Block Copolymer Composition Drives Function of Self-assembled Nanoparticles for Delivery of Small-Molecule Cargo

Caitlin L. Maikawa,[1] Alex Sevit,[1] Binhong Lin,[2] Rachel J. Wallstrom,[3] Joseph L. Mann,[3] Anthony C. Yu,[3] Robert M. Waymouth,[2] Eric A. Appel [ORCID][3]

[1]Department of Bioengineering, Stanford University, Stanford, California 94305
[2]Department of Chemistry, Stanford University, Stanford, California 94305
[3]Department of Materials Science & Engineering, Stanford University, Stanford, California 94305
Correspondence to: E. A. Appel (E-mail: eappel@stanford.edu)

ABSTRACT: Nanoparticles are useful for the delivery of small molecule therapeutics, increasing their solubility, *in vivo* residence time, and stability. Here, we used organocatalytic ring opening polymerization to produce amphiphilic block copolymers for the formation of nanoparticle drug carriers with enhanced stability, cargo encapsulation, and sustained delivery. These polymers comprised blocks of poly(ethylene glycol) (PEG), poly(valerolactone) (PVL), and poly(lactide) (PLA). Four particle chemistries were examined: (a) PEG-PLA, (b) PEG-PVL, (c) a physical mixture of PEG–PLA and PEG–PVL, and (d) PEG–PVL–PLA tri-block copolymers. Nanoparticle stability was assessed at room temperature (20 °C; pH = 7), physiological temperature (37 °C; pH = 7), in acidic media (37 °C; pH = 2), and with a digestive enzyme (lipase; 37 °C; pH = 7.4). PVL-based nanoparticles demonstrated the highest level of stability at room temperature, 37 °C and acidic conditions, but were rapidly degraded by lipase. Moreover, PVL-based nanoparticles demonstrated good cargo encapsulation, but rapid release. In contrast, PLA-based nanoparticles demonstrated poor stability and encapsulation, but sustained release. The PEG–PVL–PLA nanoparticles exhibited the best combination of stability, encapsulation, and release properties. Our results demonstrate the ability to tune nanoparticle properties by modifying the polymeric architecture and composition. © 2019 The Authors. *Journal of Polymer Science Part A: Polymer Chemistry* published by Wiley Periodicals, Inc. J. Polym. Sci., Part A: Polym. Chem. 2019, **57**, 1322–1332

KEYWORDS: nanoparticles; drug delivery; polymers; polymerization

INTRODUCTION Nanoparticles (NPs) are emerging as a powerful delivery system for small molecule therapeutics on account of their ability to increase solubility,[1,2] stability,[3,4] circulation time,[2] and cargo uptake by cells by taking advantage of native mechanisms.[5] They are extremely versatile and can be administered via intravenous infusion,[6] orally,[3,4,6] or can be incorporated into extended release depot formulations.[7] Control over the size, stability, and chemistry of NPs is critical for efficacious extension of circulation half-life and/or accumulation in target tissues.[8,9] Moreover, most chemotherapeutic drugs available for cancer treatment are hydrophobic small molecules such as paclitaxel, doxorubicin, tamoxifen, and flubendazole, which have poor solubility in water, even in the presence of traditional excipients. In addition, cancer therapeutics can be highly toxic when delivered in large doses,[10,11] and NPs have potential to facilitate more targeted delivery.[12–15] Amphiphilic block copolymers comprising poly(ethylene glycol) (PEG) and poly(lactide) (PLA), PEG–PLA, allow for self-assembly into different morphological configurations, including core–shell structures such as micelles or NPs, depending on the relative volume fractions of the two blocks.[5,9,16] The PEG chains on these particles have also been shown to increase circulation time by avoiding clearance by the reticuloendothelial system.[17–19] Previous studies have focused on the encapsulation of paclitaxel,[20–27] cisplatin,[28] and doxorubicin[29–31] in micelles for delivery.[32] Yet, micelles are dynamic particles where diblock copolymers undergo chain exchange between the micelle and the surrounding environment,[33] and consequently, these structures often suffer from dissociation upon entrance dilution.[9] In contrast, NPs are

Additional supporting information may be found in the online version of this article.
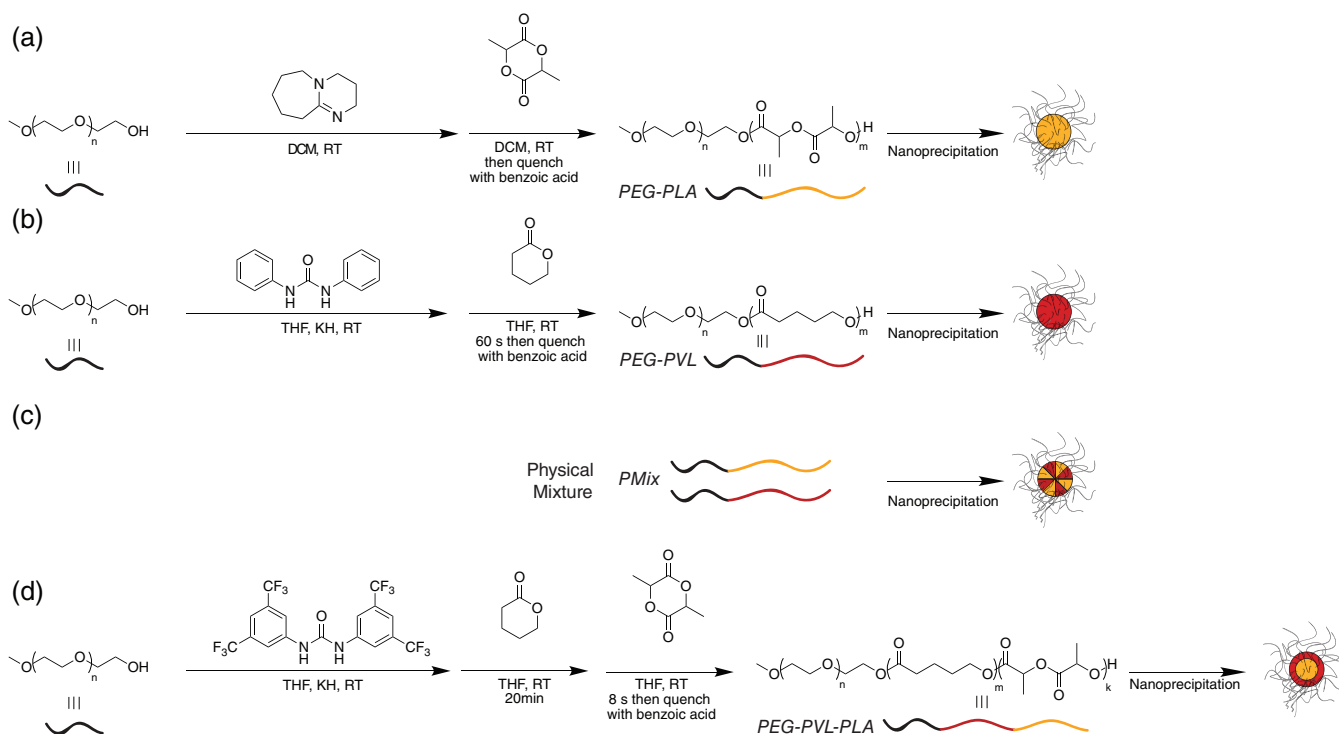
FIGURE 1 Synthetic scheme for organocatalytic ROP of block copolymers and corresponding nanoparticle chemistries (a) PEG–PLA, (b) PEG–PVL, (c) physical mixture and co-precipitation of PEG–PLA and PEG–PVL, (d) PEG–PVL–PLA. [Color figure can be viewed at wileyonlinelibrary.com]

composed of block copolymers where the hydrophobic core-forming block is high-molecular weight, enabling them to entangle and become kinetically trapped.[34] NPs with hydrophobic cores surrounded by hydrophilic shells are formed and do not suffer from dilution effects.[34] PEG–PLA NP delivery systems for paclitaxel have been investigated clinically and show promise.[35–37]

Organocatalytic ring opening polymerization (ROP) is well-suited as a method for synthesis of a broad range of biodegradable polyester polymers for use in drug delivery applications on the account of the absence of potentially toxic metal catalysts. A number of advanced organocatalytic ROP techniques have been devised, which exhibit living characteristics allowing for highly controlled polymerizations with low dispersity.[38] Indeed, the guanidine-based "superbase" 1,5,7-triazabicyclo-[4.4.0]dec-5-ene (TBD) has been previously used as a catalyst for cyclic esters such as lactide, caprolactone, or δ-valerolactone, as well as the polymerization of block copolymers of PEG with each of these monomers.[39,40] More recently, urea anion catalysts have emerged as highly selective and active catalysts for ROP that allow for high conversion of common monomers in seconds.[41] Urea anion catalysts have high tunability compared to TBD, allowing for catalyst activity to be matched to monomer reactivity by changing the substituents on the urea anions.[41] Although PEG–PLA and poly(ethylene glycol)-b-poly(valerolactone) (PEG–PVL) NPs have been extensively studied for their potential as therapeutic micelles, more complex structures have not been investigated in depth using an array of stability criteria as well as cargo encapsulation and release.[20,39,42,43] To broaden the

scope of potential therapeutic applications, new NPs with tunable release properties must be developed.

Therapeutic NPs are exposed to a variety of physiological environments depending on their target and delivery method. Long-term stability at physiological temperature may be advantageous for applications in extended controlled drug release, whereas stability and the ability to protect cargo at low pH and in the presence of proteolytic enzymes are more critical for oral delivery. In this study, we investigated the tunability of polymer NPs by altering the material composition and molecular architecture. We observed stability, cargo encapsulation and release properties of four NP carriers comprising self-assembled amphiphilic block copolymers. Block co-polymers were prepared by advanced organocatalytic ROP techniques with defined molecular weights and architectures and used to create kinetically trapped NPs by nanoprecipitation. Blocks of poly(ethylene glycol) (PEG), poly(lactide) (PLA), and poly-valerolactone (PVL) were used to make the following block copolymers for NP formation: (a) PEG–PLA, (b) PEG–PVL, (c) physical mixture and co-precipitation of PEG–PLA and PEG–PVL block co-polymers (PMix), or (d) PEG–PVL–PLA tri-block polymers (Fig. 1). NP stability was evaluated under four conditions: room temperature (20 °C; pH = 7), physiological temperature (37 °C; pH = 7), acidic condition (37 °C; pH = 2), and digestive enzyme (lipase; 37 °C; pH = 7.4). The drug release properties with both hydrophilic and hydrophobic model cargo were compared. In this study, we examined how block copolymer composition has an important role in maximizing cargo

ORIGINAL ARTICLE

WWW.POLYMERCHEMISTRY.ORG

JOURNAL OF
POLYMER SCIENCE

Polymer
Chemistry

loading, release and particle stability so that NP properties can be optimized for a wide range of applications.

EXPERIMENTS

Materials

Poly(ethylene glycol) methyl ether 5000 Da (PEG$_{5k}$; Sigma Aldrich); *rac*-lactide (99%, Alfa Aesar); δ-valerolactone (389579, Sigma Aldrich); oil Red O (Sigma Aldrich); fluorescein (Sigma Aldrich); 1,8-diazabicyclo(5.4.0)undec-7-ene (DBU) (98%, Sigma Aldrich); dimethylformamide (DMF) (99.7%, Alfa Aesar); dichloromethane (DCM) (99.8%, Sigma Aldrich); tetrahydrofuran (THF) (99.9%, Fisher Scientific); acetone (99.5%, Sigma-Aldrich); acetonitrile (99.5%, Fisher Scientific); Tween 20 (Sigma Aldrich); phosphate-buffered saline (pH ~7.4, Corning); 1,3-diphenylurea (as synthesized by Lin et al.[41]); potassium hydride (KH) (30% wt. in mineral oil, Sigma Aldrich); and benzoic acid (99.5%, Sigma Aldrich).

General Synthesis of PEG–PLA Block Copolymers

A solution of the catalyst and initiator was prepared by dissolving DBU (10.6 mg, 0.069 mmol) and PEG$_{5k}$ (250 mg, 0.050 mmol) in DCM (1 mL) in a 20 mL vial equipped with a stir bar. In a separate vial, *rac*-lactide (1.0 g, 6.9 mmol) was dissolved in DCM (3 mL) with mild heating, which was then added to the catalyst/initiator solution. The reaction was stirred for 15 minutes before quenching with excess benzoic acid. The product was recovered by precipitation from a diethyl ether:hexane (1:1) solution, collected by centrifugation, and dried under vacuum.

General Synthesis of PEG–PVL Block Copolymers

In an N$_2$-filled glovebox, a stock solution of the catalyst and initiator was prepared by dissolving KH (4.2 mg, 0.104 mmol), 1,3-diphenylurea (66.2 mg, 0.312 mmol) and PEG$_{5k}$ (520 mg, 0.104 mmol) in THF (2.1 mL), which was mildly heated to help dissolve the PEG. After the bubbling (the reaction of KH and urea generates H$_2$ gas) stopped, 2 mL of the stock solution was added via a syringe to δ-valerolactone (1.84 g, 18.4 mmol) in THF (16 mL) in a 20 mL vial equipped with a stir bar. After 60 s, a solution of benzoic acid (excess) was added to quench the reaction. The sample was removed from the glovebox for analysis. The product was purified by precipitation from a diethyl ether:hexane (1:1) solution and collected by centrifugation. The final product was dried under vacuum.

General Synthesis of PEG–PVL–PLA Block Copolymers

In an N$_2$-filled glovebox, a stock solution of the catalyst was prepared by dissolving of KH (4.8 mg, 0.12 mmol) and of 1,3-di (3,5-bistrifluoromethylphenyl)urea (116.2 mg, 0.24 mmol) in 1.4 mL of THF. The mixture was stirred until the bubbling (the reaction of KH and urea generates H$_2$ gas) stopped. A solution of initiator and monomer was prepared by dissolving PEG$_{5k}$ (400 mg, 0.08 mmol) and δ-valerolactone (VL) (890 mg, 8.9 mmol) in THF (3 mL) in a 20 mL vial equipped with a stir bar, which was then mildly heated to help dissolve the PEG. A solution of lactide was prepared by dissolving *rac*-lactide (LA) (900 mg, 8.9 mmol) in THF (3.9 mL). To begin the polymerization, 1 mL of the catalyst stock solution was added to the

PEG/VL solution. After 20 minutes (87% conversion of VL), 4 mL of the *rac*-lactide solution was immediately added to the reaction mixture. After 8 s, a solution of benzoic acid (excess) was added to quench the reaction. The sample was removed from the glovebox for analysis. The product was purified by precipitation from a diethyl ether:hexane (1:1) solution and collected by centrifugation. The final product was dried under vacuum.

Polymer Characterization

After polymer synthesis, ^{1}H nuclear magnetic resonance (NMR) was performed using an Inova 300 to obtain number-average molecular weight (M_n). All samples were characterized in D-chloroform. Absolute molecular weight and polydispersity was determined in the ASTRA software package (Wyatt Technology Corporation) after passing through two size exclusion chromatography columns (Resolve Mixed Bed Low DVB, ID 7.8 mm, Mw range 200–600,000 g mol^{-1} (Jordi Labs)) in a mobile phase of *N,N*-dimethylformamide (DMF) with 0.1 M LiBr at 35 °C and a flow rate of 1.0 mL min^{-1} (Dionex Ultimate 3000 pump, degasser, and autosampler (Thermo Fisher Scientific). Detection consisted of a Optilab T-rEX (Wyatt Technology Corporation) refractive index detector operating at 658 nm and a HELEOS II light scattering detector (Wyatt Technology Corporation) operating at 659 nm. dn/dc values for PEG, PVL, and PLA (respectively, 0.0442, 0.0495, and 0.019) in the mobile phase were calculated using $\left(\frac{dn}{dc}\right)_{ab} = \left(\frac{dn}{dc}\right)_a (wt\%)_a + \left(\frac{dn}{dc}\right)_b (wt\%)_b$ after determining the dn/dc values for PEG, PEG–PLA, PEG–PVL, and PEG–PVL–PLA polymers of known weight fractions (via ^{1}H-NMR spectroscopy) in the ASTRA software package by batch injection of three samples of known concentrations into an Optilab T-rEX refractive index detector.

NP Formation

NP self-assembly and cargo encapsulation was performed by nanoprecipitation. Polymers were dissolved in 1 mL DMF (PEG–PLA), acetone (PEG–PVL), or acetonitrile (PEG–PLA–PVL, PEG–PLA/PEG–PVL). Polymer solution was added dropwise to 10 mL deionized water stirred at 500 rpm. Particles were centrifuged in centrifugal filters (Amicon Ultra: 15 mL, MWCO 10 000) at 4500 RCF for 1 hour to concentrate the solution (concentrated to 100 μL). The NP solution was diluted to 15 wt % in deionized water.

NP Characterization

Differential scanning calorimetry (DSC) was performed using a TA Instrument Q2000 with autosampler whereby polymer (5 mg) was heated at 10 °C/min from 90 °C and 200 °C. Glass transition temperatures of each NP group were determined. Dynamic light scattering (DLS) (DynaPro II plate reader, Wyatt Technology) was used to determine hydrodynamic diameter of each NP group.

In vitro Stability Study

Particles were incubated under four conditions: room temperature (deionized water), 37 °C (deionized water), acidic conditions (HCl at pH = 2, 37 °C), and digestive enzyme (Lipase; 51 kU/L in PBS; 37°C) at 15% wt/wt. Particle size measurements were taken on day 0 and weekly over 12 weeks using dynamic light

JOURNAL OF
POLYMER SCIENCE

Polymer
Chemistry

WWW.POLYMERCHEMISTRY.ORG

ORIGINAL ARTICLE

scattering (DLS) (DynaPro II plate reader, Wyatt Technology) to measure hydrodynamic diameter of an aliquot diluted to 0.15% wt. The ratio of particle size after incubation to initial particle size was calculated.

Drug Encapsulation

NPs were prepared as described above but ORO or fluorescein (1 mg, 2% wt; 3 mg, 6% wt; and 5 mg, 10% wt relative to polymer) was dissolved in the solvent with the copolymer. After nanoprecipitation, ORO particles were filtered to remove any aggregated ORO and then diluted to a 1:3 NP solution to DMSO to release ORO trapped in the particle core. Samples were briefly vortexed. Encapsulation of the four NP groups was then measured against a standard curve using spectrophotometry (λ = 518 nm). Encapsulation efficiency was calculated by dividing the amount of ORO encapsulated by the amount of ORO added initially.

For fluorescein particles, after nanoprecipitation, particles were centrifuged in centrifugal filters (Amicon Ultra: 15 mL, 10 kDa MWCO) at 4500 RCF for 1 hour to concentrate the solution and remove non-encapsulated fluorescein. The fluorescein concentration of the filtered solution was measured against a fluorescein standard curve (λ_{Ex} = 460 nm, λ_{Em} = 550 nm). To calculate encapsulation efficiency, the difference between added fluorescein and fluorescein present in the filter flow was divided by the amount of fluorescein added initially.

Particle size of drug-loaded particles were determined immediately after nanoprecipitation (ORO) or centrifugation (Fluorescein) using dynamic light scattering (DLS) (DynaPro II plate reader, Wyatt Technology) to measure hydrodynamic diameter of an aliquot diluted to 0.15% wt.

In vitro Release Experiment

NPs were prepared as described above but ORO or fluorescein (1 mg, 2% wt relative to polymer) was dissolved in the solvent with the copolymer. The amount of ORO or fluorescein encapsulated was determined as described above. Drug-loaded particles were incubated at 37 °C for 12 weeks (ORO) or 3 weeks (Fluorescein) under sink conditions in release media (PBS with 2% Tween). Specifically, 200 μL of particles (250 mg/mL) were placed into a dialysis cup (Thermo Scientific Slide-A-Lyzer MINI Dialysis Devices, MWCO = 10 kDa) in a 24-well plate well with 2 mL of release media per well. At time points, the dialysis cup was transferred to a new well with a fresh 2 mL of release media and the old release media was used to determine release. For ORO

release, media was replaced weekly and ORO release was measured against a standard curve using a BioTek SynergyH1 microplate reader (λ = 518 nm). For fluorescein release, media was replaced at each time point (sampling frequency decreased over time). The fluorescein concentration in the release media was measured using spectroscopy against a fluorescein standard curve (λ_{Ex} = 460 nm, λ_{Em} = 550 nm). The cumulative amount of drug released at each time point was calculated.

RESULTS

Block Co-Polymer Synthesis and NP Formation

Block copolymers PEG–PLA, PEG–PVL, and PEG–PVL–PLA were synthesized using organocatalytic ROP with a urea anion catalyst as shown in Figure 1. The PEG–PVL–PLA tri-block copolymer was prepared by sequential addition of δ-valerolactone and lactide. It should be noted that because of the differences in reactivity between lactide and δ-valerolactone, PEG–PVL–PLA is the only possible sequence of blocks. Lin et al. observed that lactide has a polymerization rate orders of magnitude faster than δ-valerolactone when polymerized with the urea anion catalyst.[41] A PEG–PLA–PVL polymer is not possible using these methods on account of extensive back-biting within the PLA block.

Each of the polymers prepared for this study were characterized using nuclear magnetic resonance (NMR) spectroscopy and gel permeation chromatography (GPC), and values are reported in Table 1. The organocatalytic ROP technique utilized here produces polymers with narrow dispersity ($Đ_{PEG - PVL}$ = 1.04; $Đ_{PEG - PVL - PLA}$ = 1.10; $Đ_{PEG - PLA}$ = 1.13), which is similar to the results ($Đ \sim 1.06$–1.10) reported by Lin et al. in previous studies.[41] ^{1}H-NMR was used to determine copolymer molecular weight, clearly showing the expected peaks for the individual block components of the polymers (i.e., PEG protons at 3.63 ppm, PVL protons at 4.08 ppm, and PLA protons at 5.16 ppm; Supporting Information Fig. S2–S6). Molecular weights for all complete block copolymers prepared ranged from M_n = 24.6 kDa to 27.3 kDa by NMR for a target molecular weight of M_n = 25 kDa. A target molecular weight of 25 kDa allows for the hydrophobic portions of polymer chains to self assemble to form a kinetically trapped entangled core. Furthermore, GPC analysis indicates a clean shift in the molecular weight from PEG to PEG–PVL to PEG–PVL–PLA upon addition of each subsequent block (Fig. 2).

With block copolymers in hand, we sought to produce NPs using standard approaches to nanoprecipitation. A series of four NPs

TABLE 1 Characteristics of PEG–PLA, PEG–PVL, PMix, and PEG–PVL–PLA Copolymers and Nanoparticles

Polymer	M_n[a] (kDa)	M_n[b] (kDa)	$Đ$[b]	D_h[c] (nm)	Polydispersity[c] (PD)	$T_{g\ PLA}$[d] (°C)	$T_{g\ PVL}$[d] (°C)
PEG–PLA	24.6	29.0	1.13	57.6	0.22	14	n/a
PEG–PVL	27.3	29.4	1.04	49.6	0.23	n/a	−81
PMix	–	–	–	41.5	0.09	15	−79
PEG–PVL–PLA	25.9	24.4	1.10	39.4	0.13	14	−79

[a] Determined with ^{1}H-NMR.
[b] Determined with multi angle light scattering (MALS) and dn/dc values.
[c] Determined with dynamic light scattering.
[d] Determined with differential scanning calorimetry.
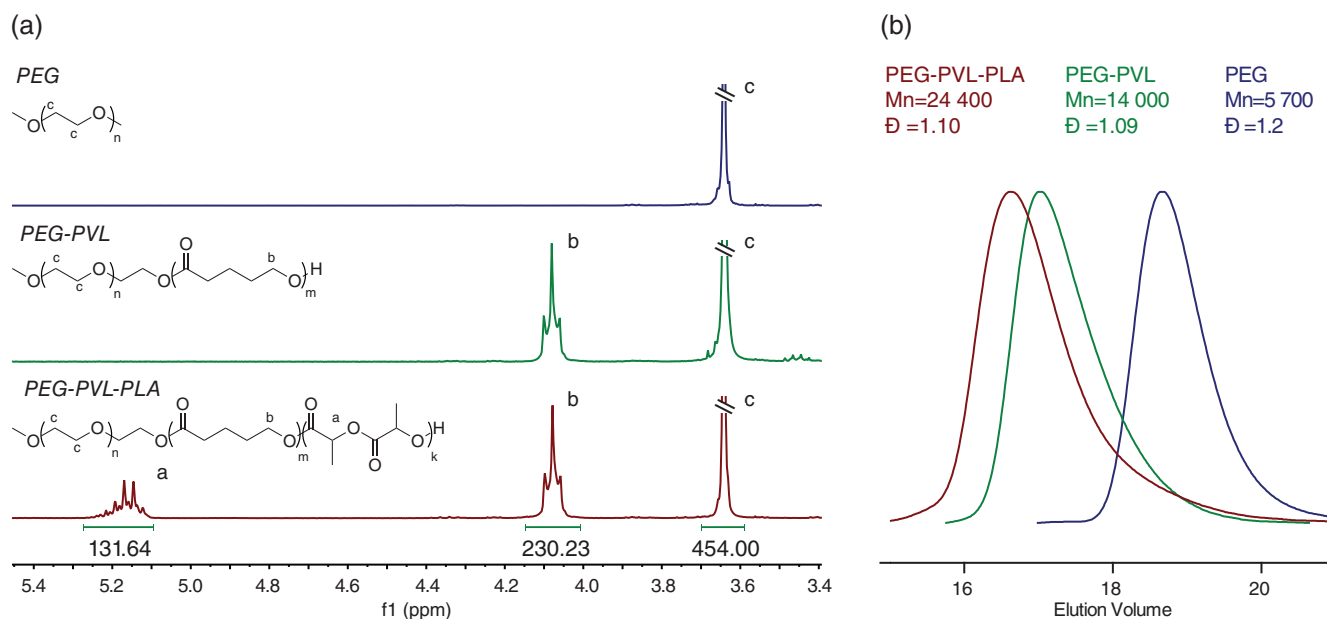
FIGURE 2 Characterization of tri-block PEG–PVL–PLA co-polymers: (a) ^{1}H NMR spectra in D-chloroform at 300 MHz and (b) GPC traces of PEG (blue), PEG–PVL intermediate (green), and PEG–PVL–PLA (red). [Color figure can be viewed at wileyonlinelibrary.com]

were prepared: (a) PEG–PLA, (b) PEG–PVL, (c) physical mixture of PEG–PLA and PEG–PVL (PMix), and (d) PEG–PVL–PLA. The choice of solvent used in the nanoprecipitation process has been shown to strongly impact the size of the resulting NPs.[22] We therefore screened several solvents, including DMF (PEG–PLA), acetone (PEG–PVL), and acetonitrile (PMix and PEG–PVL–PLA), to obtain NPs of similar size across each of the groups. NP fabrication yield for the nanoprecipitation process was $83 \pm 2\%$ (data not shown). Hydrodynamic diameter for each of the NPs was determined with DLS and were found to fall between 39.4 and 57.6 nm (Table 1). NP size dispersity was between 0.09 and 0.23 (Table 1), similar to previous observations in the literature using this method.[22]

The glass transition temperature (T_g) was measured for each of the NPs following lyophilization. The T_gs were taken from the second heat cycle of the DSC. PLA T_g was between 14 and 15 °C and PVL T_g was between −81 and −79 °C. Interestingly, two distinct T_gs exist for PMix and PEG–PVL–PLA NPs corresponding to PLA and PVL, likely arising because PLA and PVL are not miscible and can phase segregate in the NP core. Zeta-potential of the particles was measured (Supporting Information Fig. S1). PEG–PLA particles and PEG–PVL–PLA particles were negatively charged (PEG–PLA: −21 ± 1 mV; PEG–PVL–PLA: −9.3 ± 0.3 mV), and PEG–PVL and PMix particles were approximately neutral (PEG–PVL: −2.0 ± 0.7 mV; PMix: 1.6 ± 1 mV).

In vitro Stability
Particle diameter, measured with dynamic light scattering (DLS), was used as a metric of NP stability over time under several distinct test conditions: (a) room temperature (20 °C; pH = 7.4), (b) physiological temperature (37 °C; pH = 7), (c) acidic media (pH = 2; 37 °C), and (d) in the presence of a digestive enzyme (lipase; pH = 7.4; 37 °C) (Fig. 3). Here, we evaluated NPs for 12 weeks to

probe NP properties under a range of test conditions. Although gastric residence time is on the order of hours, our intent was to use acidic media and lipase exposure as model systems to understand the effects these particles under stressed conditions. NPs were between 39.4 and 57.6 nm in diameter on day 0 (Table 1), and no change in particle diameter was observed across all NP groups incubated at room temperature for the entire duration of the 12-week study [Fig. 3(a)]. These observations suggest that all NPs exhibit a high degree of stability [Fig. 3(a)]. Lin et al. have previously showed similar stability for NPs comprising PEG–PLA and PEG–PVL at 4 °C.[39] In contrast, we have shown that temperature affects long-term stability of PEG–PLA and PMix NPs, whereby these NPs agglomerated at physiological temperatures (37 °C), resulting in increased mean NP diameters with more disperse size distributions after 7 weeks, 8 weeks, and 11 weeks for PEG–PLA, PMix, and PEG–PVL–PLA NPs, respectively. PEG–PVL NPs remained stable for the entire duration of the 12-week study [Fig. 3(b)].

In acidic media (pH = 2; 37 °C), PEG–PVL NPs remained stable, but PEG–PLA, PMix, and PEG–PVL–PLA NPs showed a greater than twofold increase in diameter after 7, 8, and 9 weeks, respectively [Fig. 3(c)]. The onset of size instability in PEG–PLA and PMix NPs occurred at a similar time point in both 37 °C and acidic conditions (also incubated at 37 °C) suggests that PEG–PLA degradation may be linked to temperature. It is unclear whether the formulation at pH = 2 or storage at 37 °C is the dominant factor for instability of these NPs under these conditions.

We also assessed NP stability in the presence of lipase (50,900 U/L; pH = 7.4; 37 °C) at concentrations comparable to physiological concentrations found in the stomach.[44] Interestingly, PEG–PVL showed rapid increases (>15-fold) in diameter after 1 week under these enzymatic conditions. PEG–PVL–PLA
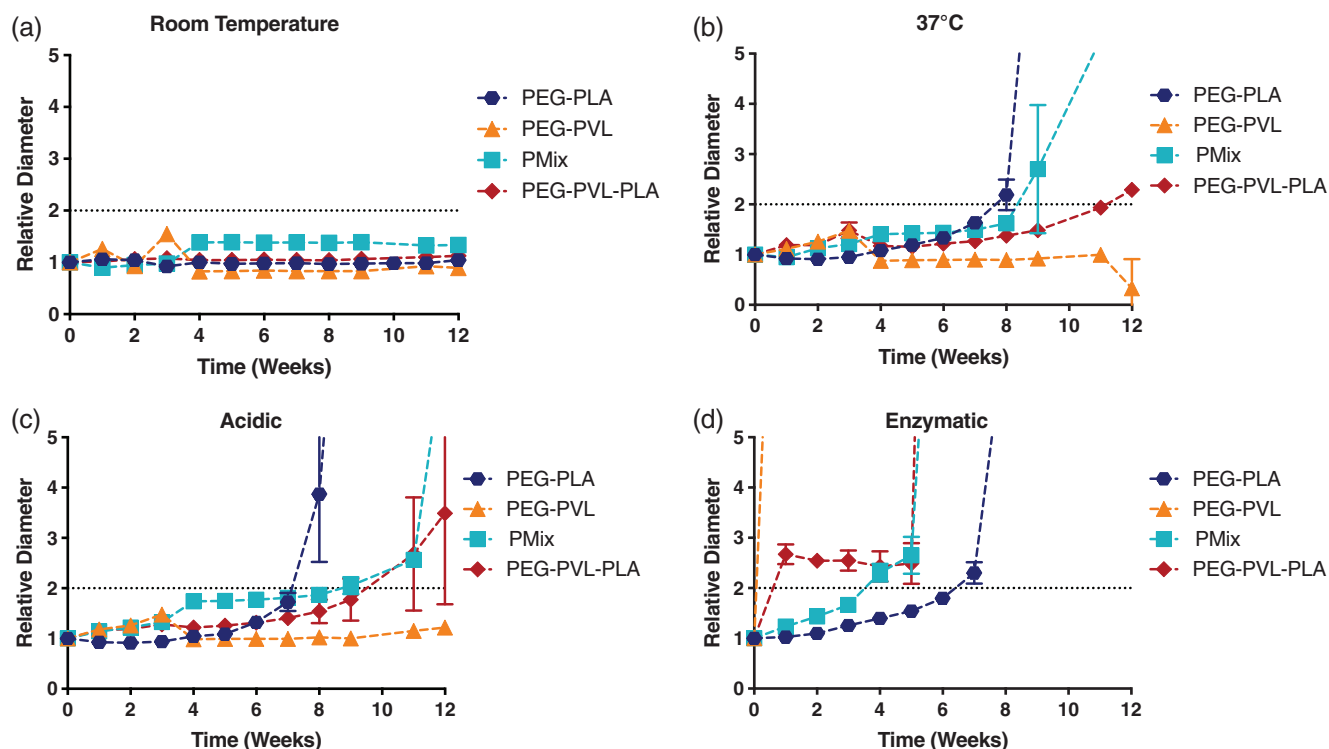
FIGURE 3 Nanoparticle stability as relative particle diameter over 12 weeks of PEG–PLA, PEG–PVL, PMix, and PEG–PVL–PLA nanoparticles exposed to four incubation conditions: (a) room temperature; (b) 37 °C; (c) acidic condition (pH = 2; 37 °C); (d) digestive enzyme (lipase; 51kU/L; 37 °C). Data expressed as mean $\pm$ standard deviation (s.d.) (n = 3) [Color figure can be viewed at wileyonlinelibrary.com]

particles showed an initial size increase but then stabilized around 2.5-fold their initial diameter. PEG–PLA and PEG–PVL–PLA NPs retain the highest level of stability after incubation with lipase, showing instabilities after 6 weeks and 5 weeks, respectively, whereas PMix NPs remained stable for 3 weeks.

Through these four studies, we observed that PMix and PEG–PLA NPs exhibited similar stability profiles. In comparison, PEG–PVL and PEG–PVL–PLA NPs showed generally superior stability; however, PEG–PVL showed rapid degradation under enzymatic conditions, whereas PEG–PVL–PLA showed increased enzymatic stability in comparison to PEG–PVL. These studies indicate the following stability hierarchy within these materials: PMix ~ PEG–PLA << PEG–PVL < PEG–PVL–PLA.

Cargo Encapsulation

We investigated model cargo encapsulation using Oil Red O (ORO) (log$P$ = 9.81)[45] as a model hydrophobic cargo. PEG–PVL NPs had the highest encapsulation efficiencies. Of the studies targeting NP loading of 2% w/w ORO with respect to polymer, the PEG–PVL and PEG–PVL–PLA NPs showed the highest loading efficiency of 0.93 $\pm$ 0.13 and 0.94 $\pm$ 0.18, respectively, whereas the loading efficiency of PEG–PLA (0.76 $\pm$ 0.09) and PMix (0.76 $\pm$ 0.06) NPs was lower. These results suggest that the amount of ORO that can be encapsulated is strongly impacted by the intermolecular interactions with the hydrophobic core. A trend of decreasing encapsulation efficiency with increased ORO loading was observed across groups; however, this trend was most prominent in PMix and

PEG–PVL–PLA groups [Fig. 4(a)]. PEG–PVL maintained the highest loading efficiency 0.81 $\pm$ 0.03 at 10% w/w, whereas PEG–PLA, PMix, and PEG–PVL–PLA NPs exhibited 0.65 $\pm$ 0.03, 0.39 $\pm$ 0.01, and 0.51 $\pm$ 0.06 w/w loading, respectively. These results suggest that PEG–PVL NPs have a greater capacity to encapsulate hydrophobic small molecules at 10% (w/w) loading concentrations.

We also investigated encapsulation using fluorescein (log$P$ = 3.86)[46] [Fig. 4(b)]. The trends observed for fluorescein encapsulation were similar to those observed for ORO encapsulation. PEG–PVL and PEG–PVL–PLA NPs showed the highest loading efficiency at 2% w/w fluorescein at 0.97 $\pm$ 0.01 and 0.964 $\pm$ 0.005, respectively. PMix and PEG–PLA NPs exhibited loading efficiencies of 0.76 $\pm$ 0.01 and 0.50 $\pm$ 0.04, respectively. PEG–PVL retained the highest loading efficiency up to 10% w/w fluorescein (0.76 $\pm$ 0.04) compared to PEG–PLA (0.51 $\pm$ 0.01), PMix (0.16 $\pm$ 0.08), and PEG–PVL–PLA (0.59 $\pm$ 0.09). PMix NPs showed decreased loading efficiency at fluorescein loadings above 2% compared to other NP compositions, with 0.10 $\pm$ 0.10 at 6% fluorescein and 0.16 $\pm$ 0.08 at 10% fluorescein. These results suggest that PEG–PVL and PEG–PVL–PLA NPs have the greatest capacity to encapsulate cargo with intermediate log$P$ values, especially at 2%–6% (w/w) loading concentrations.

In these studies, we observed that PMix NPs showed the lowest encapsulation efficiency, whereas PEG–PVL and PEG–PVL–PLA NPs had similarly high levels of encapsulation, whereby encapsulation characteristics exhibited the following trend: PMix < PEG–PLA < PEG–PVL ~ PEG–PVL–PLA.
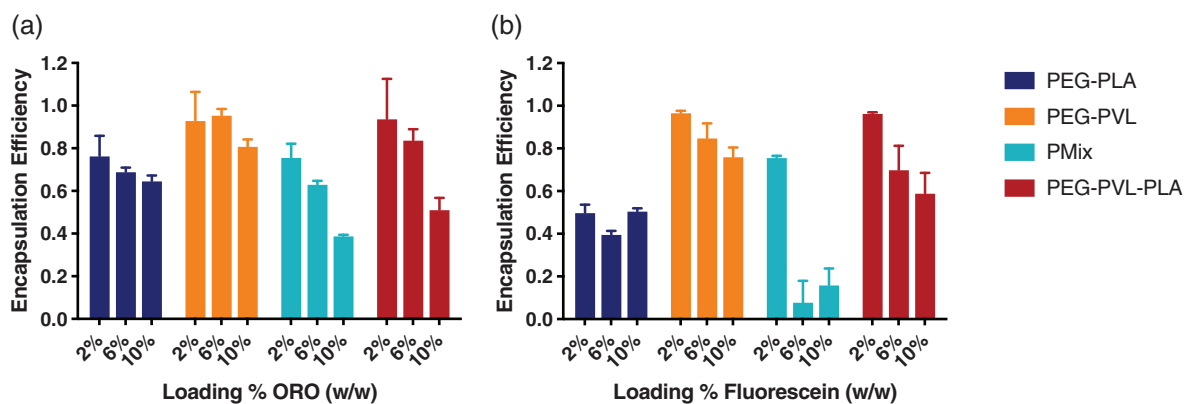
FIGURE 4 Encapsulation efficiency at 2% wt loading, 6% wt loading, and 10% wt loading with respect to the polymer for (a) ORO and (b) fluorescein loading into PEG–PLA, PEG–PVL, PMix, and PEG–PVL–PLA NPs during nanoprecipitation. Data expressed as mean ± standard deviation ($n = 3$) [Color figure can be viewed at wileyonlinelibrary.com]

In vitro Cargo Release

ORO release from PEG–PVL, PMix, and PEG–PVL–PLA NPs appeared to be roughly zero-order in nature for the duration of the 12 week study (Fig. 5). It was expected that the highly hydrophobic nature of the model cargo would result in slow release as the polymer chains hydrolytically erode into the release media. Batycky et al. describe that in the release of hydrophobic cargo, hydration and erosion change the pore size within the particle over time, allowing for the release of the cargo after an induction period.[47] In this model, the radius of the particle is assumed to remain unchanged during the erosion process. This assumption is consistent with our stability data, which indicated that there is no change in particle diameter in all NP groups tested for at least 7 weeks, when PEG–PLA and PMix NPs began to agglomerate. The release curves (Fig. 5) suggest an induction period before erosion-driven release begins. Mean induction time appears to range between 0 and 3 weeks, with the longest induction time seen for PEG–PVL–PLA particles (3 ± 2 weeks). Data points after induction time were fit with the Korsmeyer-
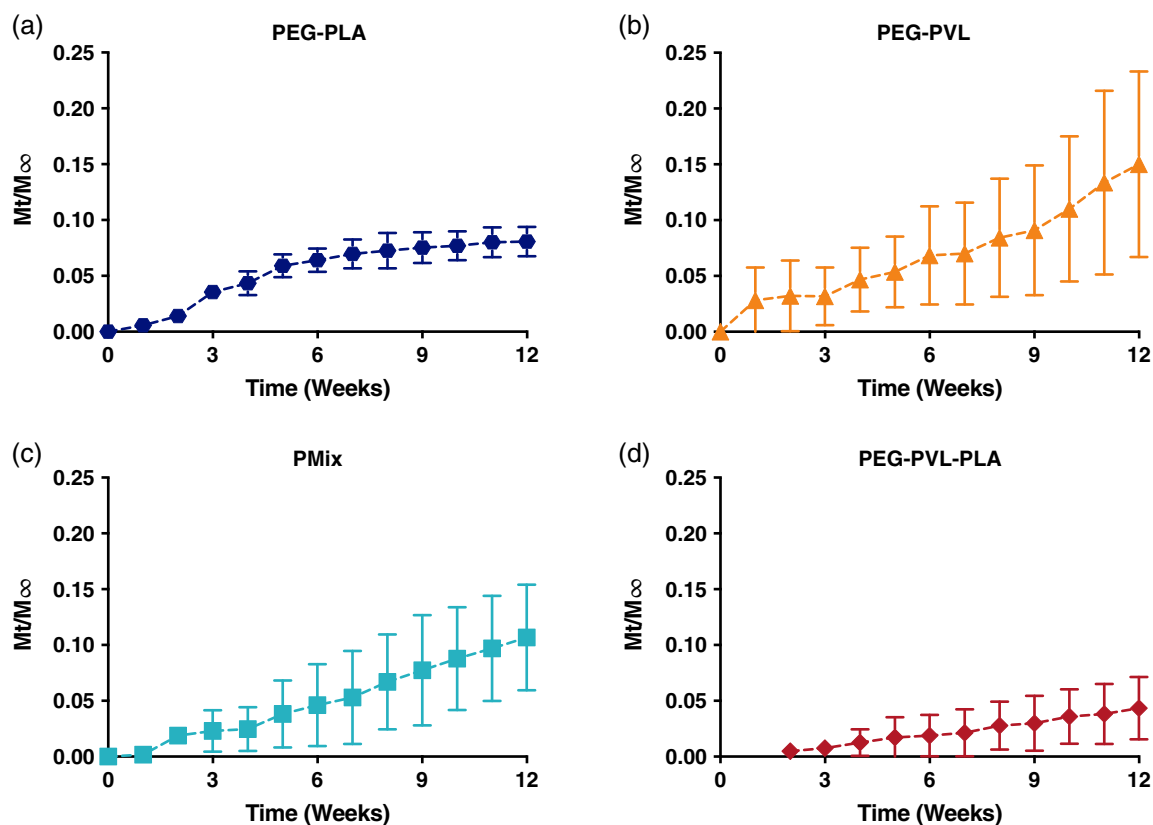

FIGURE 5 In vitro ORO release from (a) PEG–PLA, (b) PEG–PVL, (c) PMix, and (d) PEG–PVL–PLA nanoparticles over 12 weeks. Data expressed as mean ± standard deviation ($n = 3$) [Color figure can be viewed at wileyonlinelibrary.com]

TABLE 2 Korsmeyer-Peppas Release of ORO and Fluorescein-Loaded NPs

Polymer	ORO			Fluorescein		
	Induction (weeks)	k (day$^{1/n}$)	n	D (nm^2/day)	k (day$^{1/n}$)	n
PEG–PLA	0 ± 0	0.012	1.1	20.6	0.092	0.90
PEG–PVL	1 ± 1	0.021	0.8	13.1	0.10	0.74
PMix	1 ± 1	0.0016	1.4	14.7	0.15	0.74
PEG–PVL–PLA	3 ± 2	0.0045	1.2	16.2	0.16	0.67

Peppas release equation, and all NPs had n values of approximately 1, suggesting erosion is the primary mode of release (Table 2).[48,49] PEG–PVL–PLA NPs showed decreased cumulative release compared to the other groups over the course of the 12-week study. This observation may result from the prolonged stability of PEG–PVL–PLA NPs combined with the longer 3-week induction time observed before release begins. Release of ORO from PEG–PLA NPs exhibited steady release for the first 6 weeks followed by stagnation after approximately 6 weeks. The timing of the decrease in ORO release rate at approximately 6 weeks correlates with the onset of PEG–PLA NP instability observed in the degradation studies discussed above, suggesting that NP aggregation may impede the release of ORO into the media. Although these studies were not continued beyond 12 weeks, it is expected that consistent release from NPs would continue. Because ORO release did not reach a plateau region during this 12 week period, we reflect M_∞ as the reported encapsulation efficiency.

Fluorescein release from each of the NPs was measured over a 5 week period (Fig. 6). It has previously been reported that burst release is expected when diffusion is the predominant release mechanism.[50] Accordingly, we expected that fluorescein, which has a log$P$ value that favors the aqueous phase, would diffuses rapidly out of the NPs into the surrounding aqueous release media. The first 60% of fluorescein release was initially analyzed using the Korsmeyer-Peppas release equation.[48,51] NPs exhibited n values ranging from 0.7 to 0.9, which is within the range for anomalous release from a sphere (Table 2). It was expected that the relative hydrophilicity of fluorescein would cause release to be primarily by diffusion, but the anomalous release observed here suggests a combination of diffusion and erosion. Ritger et al. state that although the generalized power law equation can be used for non-planar geometries, the interpretation of the n and k parameters may be affected.[51] To further characterize the release of hydrophilic cargo from the NPs, Ritger-Peppas fickian
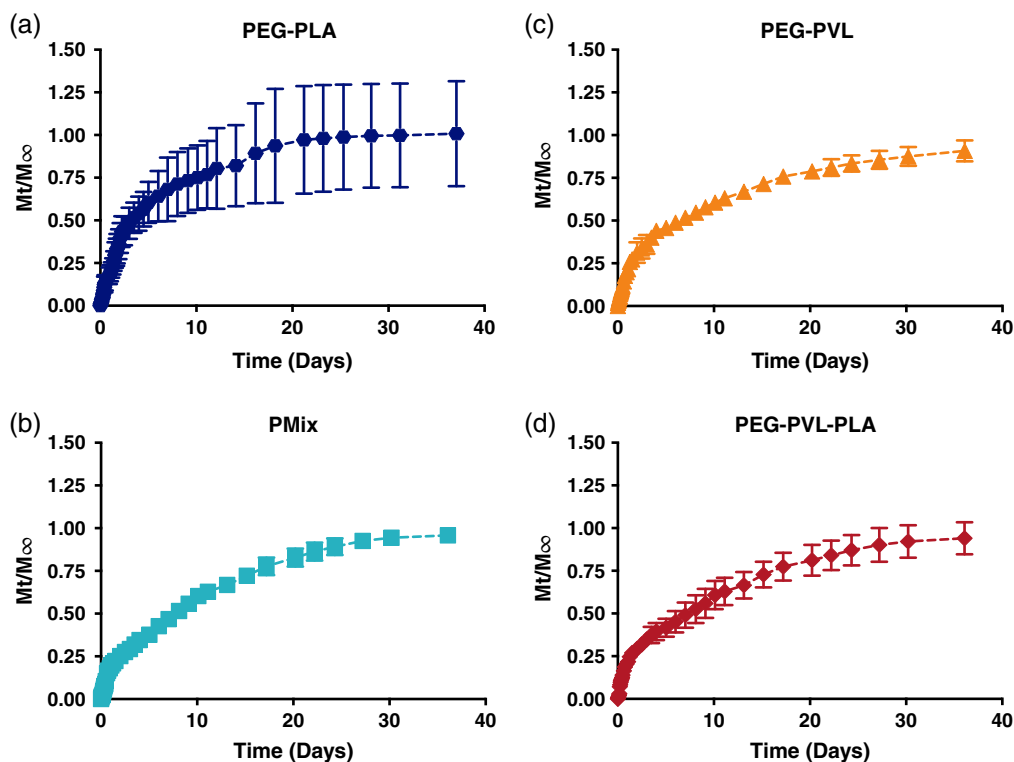

FIGURE 6 *In vitro* fluorescein release from (a) PEG–PLA, (b) PEG–PVL, (c) PMix, and (d) PEG–PVL–PLA nanoparticles over 5 weeks. Particles were incubated in pH = 7.4 phosphate-buffered saline at 37 °C. Data expressed as mean $\pm$ standard deviation ($n = 3$) [Color figure can be viewed at wileyonlinelibrary.com]

diffusion from a sphere was also used to model the data.[51] The diffusion coefficient ranged from 13.1 to 20.6 nm^2/day for all NP groups (Table 2). In these studies, M_∞ is not reflective of measured loading efficiencies for fluorescein and is adjusted such that release curves approach 1.0 at t_∞. It is possible that some degree of self-quenching may occur with entrapped fluorescein and that fluorescein loading in NPs was overestimated. Cumulative release after 5 weeks based on loading efficiency values were 0.40 ± 0.10 for PEG–PLA, 0.64 ± 0.04 for PEG–PVL, 0.48 ± 0.02 for PMix, and 0.56 ± 0.06 for PEG–PVL–PLA NPs. Here, M_t/M_∞ was determined to be 0.4, 0.7, 0.5, and 0.6 for PEG–PLA, PEG–PVL, PMix, and PEG–PVL–PLA NPs, respectively.

DISCUSSION

In this study, we demonstrate that polymer NP stability, cargo loading, and release properties can be enhanced through alteration of composition and architecture of the polymers used to prepare them. NPs are exposed to a range of conditions in various therapeutic applications and understanding the critical design criteria underlying structure–property relationships along multiple axis (e.g., cargo encapsulation, stability under diverse conditions) will enable the development of NPs that are optimal for their intended function.

NP stability can be tuned with polymer composition and structure for optimal performance under different environmental conditions. Based on the observed stability of NP groups in this study, it appears that the PLA component of the PMix NPs may account for the similar pattern of instability onset between the PEG–PLA and PMix groups. In contrast, the PVL component of the PEG–PVL–PLA copolymer appears to contribute to a large increase in NP stability. In the PEG–PVL–PLA NPs, the PVL portion of the tri-block copolymer connects directly to the PEG chain of the hydrophilic corona of the NPs. For this reason, it is likely that the outer surface of the PEG–PVL–PLA hydrophobic core is primarily composed of PVL, which may act as a protective shield for the PLA component in the 37 °C and acidic conditions. PVL chains have fewer ester functional groups per monomer and are more hydrophobic, making them less susceptible to hydrolysis than PLA chains. This feature may explain the prolonged stability observed for PEG–PVL and PEG–PVL–PLA NPs when compared to PEG–PLA and PMix NPs. Under lipase conditions, however, PEG–PVL NPs degraded rapidly compared to PEG–PLA NPs. Lipase is a digestive enzyme that catalyzes the hydrolysis of ester bonds in triglycerides. The heightened degradation of PEG–PVL NPs in the presence of lipase may result from decreased steric hindrance when compared to PLA, which contains methyl groups pendant from the backbone in the alpha position relative to the backbone esters, thus allowing more facile lipase access to the esters along the polymer chain.

The PVL component of the NPs exhibited improved cargo loading for both fluorescein and ORO cargo. These observations are corroborated by a report by Lin et al., where encapsulation efficiency of indomethacin, a hydrophobic anti-inflammatory drug, was observed to be significantly lower in PEG–PLA NPs than in PEG–PVL NPs.[39] The decreased encapsulation efficiency observed in
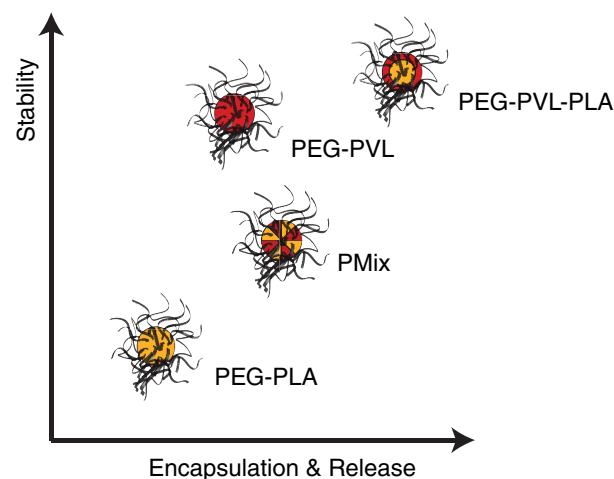

FIGURE 7 Schematic summary of stability versus release and encapsulation properties of (a) PEG–PLA, (b) PEG–PVL, (c) PMix, and (d) PEG–PVL–PLA nanoparticles. Data expressed as mean ± standard deviation ($n = 3$) [Color figure can be viewed at wileyonlinelibrary.com]

PMix NPs compared to either PEG–PLA or PEG–PVL NPs, suggests an antagonistic interaction between the cargo and the two polymer components in the physical mixture that reduces encapsulation during the nanoprecipitation process. In addition, the high encapsulation efficiencies observed at ORO loadings of 2% and 6% for both PEG–PVL and PEG–PVL–PLA NPs may be related to favorable intermolecular interactions with the PVL block in the tri-block copolymer.

The glass transition temperatures of the PVL and PLA blocks appeared to play a critical role in determining the release kinetics of molecular cargo from different NPs types. PEG–PVL NPs, which had a glass transition temperature of approximately −80 °C, exhibited the most rapid release of entrapped cargo, whereas PEG–PLA NPs, which had glass transition temperatures of approximately 15 °C, exhibited much slower cargo release. Sustained release is desirable in many applications to eliminate negative effects from burst release and to ensure release occurs over a similar time-frame as particle degradation to prevent the accumulation of particle components. PMix particles, which comprise a physical mixture of PEG–PLA and PEG–PVL, exhibited rapid release similar to PEG–PVL alone, whereas PEG–PVL–PLA NPs exhibited slow release similar to PEG–PLA alone.

Through these studies, it appear that NPs comprised of PEG–PVL–PLA tri-block copolymers exhibit synergistic contributions of PLA and PVL to enhance NP stability under numerous conditions, enhance cargo encapsulation, and slow down the release of entrapped cargo.

CONCLUSIONS

In this work, we have examined the impact of polymer composition and molecular architecture on the behavior of self-assembled

NPs. The optimal NP for therapeutic delivery will, in many cases, have cargo release rates on the same time-frame as degradation rates, such that NPs do not accumulate *in vivo* after releasing their cargo. We have shown that organocatalytic ROP techniques can provide a simple and rapid method to prepare advanced polymers enabling more effective polymeric NPs. Our results have shown that the NPs comprising PEG–PVL–PLA triblock copolymers exhibit the best combination of stability across numerous conditions, cargo encapsulation efficiency with multiple cargo, and release properties of the four NP systems evaluated (Fig. 7). The PEG–PVL–PLA NP platform appears to be robust under a variety of relevant conditions and has potential utility as a delivery vehicle for pharmaceuticals.

ACKNOWLEDGMENTS

REFERENCES AND NOTES

1 Z. Gao, A. N. Lukyanov, A. Singhal, V. P. Torchilin, *Nano Lett.* **2002**, *2*, 979.

2 J.-C. Leroux, E. Allémann, F. De Jaeghere, E. Doelker, R. Gurny, *J. Control. Release* **1996**, *39*, 339.

3 E. M. Pridgen, F. Alexis, O. C. Farokhzad, *Expert Opin. Drug Deliv.* **2015**, *12*, 1459.

4 A. A. Date, J. Hanes, L. M. Ensign, *J. Control. Release* **2016**, *240*, 504.

5 K. Cho, X. Wang, S. Nie, Z. G. Chen, D. M. Shin, *Clin. Cancer Res.* **2008**, *14*, 1310.

6 L. Yildirimer, N. T. K. Thanh, M. Loizidou, A. M. Seifalian, *Nano Today* **2011**, *6*, 585.

7 E. A. Appel, M. W. Tibbitt, M. J. Webber, B. A. Mattix, O. Veiseh, R. Langer, *Nat. Commun.* **2015**, *6*(6295), 6295.

8 A. Z. Wilczewska, K. Niemirowicz, K. H. Markiewicz, H. Car, *Pharmacol. Rep.* **2012**, *64*, 1020.

9 M. Elsabahy, K. L. Wooley, *Chem. Soc. Rev.* **2012**, *41*, 2545.

10 E. K. Rowinsky, R. C. Donehower, *N. Engl. J. Med.* **1995**, *332*, 1004.

11 L. J. Steinherz, P. G. Steinherz, C. T. Tan, G. Heller, M. L. Murphy, *JAMA* **1991**, *266*, 1672.

12 X. Xu, P. E. Saw, W. Tao, Y. Li, X. Ji, S. Bhasin, Y. Liu, D. Ayyash, J. Rasmussen, M. Huo, et al., *Adv. Mater.* **2017**, *29*, 1700141.

13 B. Yameen, W. I. Choi, C. Vilos, A. Swami, J. Shi, O. C. Farokhzad, *J. Control. Release* **2014**, *190*, 485.

14 S. Y. Tzeng, D. R. Wilson, S. K. Hansen, A. Quiñones-Hinojosa, J. J. Green, *Bioeng. Transl. Med.* **2016**, *1*, 149.

15 J. Kim, D. R. Wilson, C. G. Zamboni, J. J. Green, *J. Drug Target.* **2015**, *23*, 627.

16 J. P. K. Tan, S. H. Kim, F. Nederberg, E. A. Appel, R. M. Waymouth, Y. Zhang, J. L. Hedrick, Y. Y. Yang, *Small* **2009**, *5*, 1504.

17 D. S. Spencer, A. S. Puranik, N. A. Peppas, *Curr. Opin. Chem. Eng.* **2015**, *7*, 84.

18 J. V. Jokerst, T. Lobovkina, R. N. Zare, S. S. Gambhir, *Nanomedicine* **2011**, *6*, 715.

19 J. S. Suk, Q. Xu, N. Kim, J. Hanes, L. M. Ensign, *Adv. Drug Deliv. Rev.* **2016**, *99*, 28.

20 F. Nederberg, E. Appel, J. P. K. Tan, S. H. Kim, K. Fukushima, J. Sly, R. D. Miller, R. M. Waymouth, Y. Y. Yang, J. L. Hedrick, *Biomacromolecules* **2009**, *10*, 1460.

21 P. Ma, R. J. Mumper, *J. Nanomed. Nanotechnol.* **2013**, *4*, 1000164.

22 J. Cheng, B. A. Teply, I. Sherifi, J. Sung, G. Luther, F. X. Gu, E. Levy-Nissenbaum, A. F. Radovic-Moreno, R. Langer, O. C. Farokhzad, *Biomaterials* **2007**, *28*, 869.

23 F. Zhang, S. Zhang, S. F. Pollack, R. Li, A. M. Gonzalez, J. Fan, J. Zou, S. E. Leininger, A. Pavía-Sanders, R. Johnson, L. D. Nelson, J. E. Raymond, M. Elsabahy, D. M. P. Hughes, M. W. Lenox, T. P. Gustafson, K. L. Wooley, *J. Am. Chem. Soc.* **2015**, *137*, 2056.

24 F. Zhang, S. Khan, R. Li, J. A. Smolen, S. Zhang, G. Zhu, L. Su, A. A. Jahnke, M. Elsabahy, X. Chen, K. L. Wooley, *Nanoscale* **2017a**, *9*, 15773.

25 E. Nance, C. Zhang, T.-Y. Shih, Q. Xu, B. S. Schuster, J. Hanes, *ACS Nano* **2014**, *8*, 10655.

26 M. Yang, T. Yu, Y.-Y. Wang, S. K. Lai, Q. Zeng, B. Miao, B. C. Tang, B. W. Simons, L. M. Ensign, G. Liu, K. W. Y. Chan, C. Y. Juang, O. Mert, J. Wood, J. Fu, M. T. McMahon, T. C. Wu, C. F. Hung, J. Hanes, *Adv. Healthc. Mater.* **2014**, *3*, 1044.

27 L. Y. Lin, A. Karwa, J. G. Kostelc, N. S. Lee, R. B. Dorshow, K. L. Wooley, *Mol. Pharm.* **2012**, *9*, 2248.

28 C. Zhang, E. A. Nance, P. Mastorakos, J. Chisholm, S. Berry, C. Eberhart, B. Tyler, H. Brem, J. S. Suk, J. Hanes, *J. Control. Release* **2017b**, *263*, 112.

29 Q. Zhu, L. Jia, Z. Gao, C. Wang, H. Jiang, J. Zhang, L. Dong, *Mol. Pharm.* **2014**, *11*, 3269.

30 M. E. Davis, Z. G. Chen, D. M. Shin, *Nat. Rev. Drug Discov.* **2008**, *7*, 771.

31 L. Y. Lin, N. S. Lee, J. Zhu, A. M. Nyström, D. J. Pochan, R. B. Dorshow, K. L. Wooley, *J. Control. Release* **2011**, *152*, 37.

32 C. Salvador-Morales, W. Gao, P. Ghatalia, F. Murshed, W. Aizu, R. Langer, O. C. Farokhzad, *Expert Rev. Anticancer Ther.* **2009**, *9*, 211.

33 Y. Ma, T. P. Lodge, *Macromolecules* **2016**, *49*, 9542.

34 T. Nicolai, O. Colombani, C. Chassenieux, *Soft Matter* **2010**, *6*, 3111.

35 T.-Y. Kim, D.-W. Kim, J.-Y. Chung, S. G. Shin, S.-C. Kim, D. S. Heo, N. K. Kim, Y.-J. Bang, *Clin. Cancer Res.* **2004**, *10*, 3708.

36 K. S. Lee, H. C. Chung, S. A. Im, Y. H. Park, C. S. Kim, S.-B. Kim, S. Y. Rha, M. Y. Lee, J. Ro, *Breast Cancer Res. Treat.* **2008**, *108*, 241.

37 D.-W. Kim, S.-Y. Kim, H.-K. Kim, S.-W. Kim, S. W. Shin, J. S. Kim, K. Park, M. Y. Lee, D. S. Heo, *Ann. Oncol.* **2007**, *18*, 2009.

38 P. P. Datta, M. K. Kiesewetter, *Macromolecules* **2016**, *49*, 774.

39 W.-J. Lin, Y.-C. Chen, C.-C. Lin, C.-F. Chen, J.-W. Chen, *J. Biomed. Mater. Res. B Appl. Biomater.* **2006a**, *77*, 188.

40 B. G. G. Lohmeijer, R. C. Pratt, F. Leibfarth, J. W. Logan, D. A. Long, A. P. Dove, F. Nederberg, J. Choi, C. Wade, R. M. Waymouth, J. L. Hedrick, *Macromolecules* **2006**, *39*, 8574.

41 B. Lin, R. M. Waymouth, *J. Am. Chem. Soc.* **2017**, *139*, 1645.

42 J.-M. Rabanel, J. Faivre, S. F. Tehrani, A. Lalloz, P. Hildgen, X. Banquy, *ACS Appl. Mater. Interfaces* **2015**, *7*, 10374.

43 W.-J. Lin, C.-L. Wang, L.-W. Juang, *J. Appl. Polym. Sci.* **2006b**, *100*, 1836.

44 M. Armand, P. Borel, C. Dubois, M. Senft, J. Peyrot, J. Salducci, H. Lafont, D. Lairon, *Am. J. Physiol.* **1994**, *266*, G372.

45 C. de Koning, M. Beekhuijzen, M. Tobor-Kapłon, S. de Vries-Buitenweg, D. Schoutsen, N. Leeijen, B. van de Waart, H. Emmen, *Birth Defects Res. B Dev. Reprod. Toxicol.* **2015**, *104*, 253.

46 Z. Rankovic, *J. Med. Chem.* **2017**, *60*, 5943.

47 R. P. Batycky, J. Hanes, R. Langer, D. A. Edwards, *J. Pharm. Sci.* **1997**, *86*, 1464.

48 S. Dash, P. N. Murthy, L. Nath, P. Chowdhury, *Acta Pol. Pharm.* **2010**, *67*, 217.

49 E. P. Holowka and S. K. Bhatia, p. 355 (**2014**).

50 J. Siepmann, F. Lecomte, R. Bodmeier, *J. Control. Release* **1999**, *60*, 379.

51 P. L. Ritger, N. A. Peppas, *J. Control. Release* **1987**, *5*, 23.